Exploring the Mechanical and Chemical Properties of Cross-Linked Poly(allylamine)-hyaluronic Acid Multilayer Films Using a Chemometric Unmixing Approach

Saeid Ekrami, Fabienne Quilès, Alice Schollhammer, Xavier Bellanger, Erwan André, Grégory Francius

https://pubs.acs.org/doi/10.1021/acsapm.3c01663

Exploring the mechanical and chemical properties of crosslinked poly(allylamine)-hyaluronic acid multilayer films using a chemometric unmixing approach

Saeid Ekrami,[1] Fabienne Quilès,[1] Alice Schollhammer,[1] Xavier Bellanger,[1] Erwan André,[1] Grégory Francius[1*]

[1]Université de Lorraine, CNRS, LCPME, F-54000 Nancy, France

* corresponding author: gregory.francius@univ-lorraine.fr

Abstract

For several decades now, modulating and controlling the mechanical properties of hydrogels, and in particular exponentially growing polyelectrolyte multilayer films (PEM), have been a major challenge, given their importance for a wide range of applications including tissue engineering, implantable biomaterials and drug delivery systems. In this work, we compared the crosslinking reaction of hydrogels based on the association of poly(allylamine) (PAH) and hyaluronic acid (HA) with either 1,4-butanediol diglycidyl ether (BDDE) or divinylsulfone (DVS) at different concentrations. On the basis of infrared data analysis by means of a chemometric method, we demonstrated that the cross-linking reaction led to significant changes in their chemical features. We deciphered how the affinity of each cross linker to alcohol and amino chemical functions drives the chemical features of the PEMs. These features can be described by a linear combination of pure HA-BDDE, PAH-BDDE or HA-DVS, PAH-DVS based hydrogels with ratios of 80% and 16% for the BDDE, and 55% and 45% for the DVS reactions, respectively. Furthermore, the mechanical properties resulting from the BDDE crosslinking reaction were consistent with a high mechanical contribution of HA-BDDE as estimated by the chemometric analysis. However, this linear combination cannot be applied for DVS. Indeed, the crosslinked PEM was softer than expected regarding the chemical contributions of HA-DVS and PAH-DVS. Our results show that it is possible to control the mechanical and chemical features by the choice of the crosslinkers alone or in a mixture.

Keywords:

Hydrogel, stiffness, atomic force microscopy, cross-linking, infrared spectroscopy

Introduction

The market for antimicrobial coatings has experienced a remarkable rise for less than a decade with annual growth of over 10% each year.[1, 2] Such an increase results from the need for selective or targeted materials to prevent the colonization of surfaces by bacteria, viruses and fungi. The development of smart antimicrobial coatings is of obvious importance in manufactured systems and processes (agroindustry, water industries, etc.) as well as for biomedical applications (e.g. hospital, implants, prosthesis, etc.).[3, 4] Latest advances in materials science allows the conception of multifunctional materials with bioactive and/or antimicrobial properties generally related to their surface properties.[5, 6] Among these materials, thin films such as polyelectrolyte multilayer films and hydrogels are gaining more and more interest due to their stability in biological environments, mechanical properties, and their storage/delivery drug ability.[7, 8]

Indeed, polyelectrolyte multilayer films and hydrogels can be used as reservoirs for drug delivery in several applications including medical, antifouling and antimicrobial purposes.[6, 9] Polyelectrolyte multilayers films (denoted PEMs) are nanostructured materials that can be formed according to layer-by-layer (LbL) methods, which consists of the growth of alternating layers with opposite charges. Several studies highlighted their high efficiency in trapping antibacterial compounds either between the layers or by post-diffusion within the gel, depending on the nature of the polyelectrolyte and its physicochemical properties.[6, 10] The PEM thickness, surface, physicochemical and mechanical properties can be easily tuned by the nature of the constitutive polyelectrolytes, the construction conditions (ionic strength, temperature, etc.) and the use of cross-linking reagents.[7, 11, 12] Indeed, control of their mechanical properties is of primary importance for tissue engineering and many biomedical applications as well as foods, water and aeronautic fields.[7, 13, 14] To this end, several reagents can be used to crosslink the constitutive polyelectrolytes of the PEM through covalent or non-covalent bonds.[15, 16] For example, N-(3-Dimethylaminopropyl)-N′-ethylcarbodiimide denoted as EDC is commonly used in literature for PEMs crosslinking to regulate cells adhesion, proliferation, and differentiation.[13, 15]

Hydrogels have also been widely reported as performant multifunctional coatings and especially for drug delivery, tissue engineering, wound dressing, antifouling and antibacterial applications.[17-20] Hydrogels are a family of physically or chemically cross-linked hydrophilic polymers leading to a 3D network holding a very high-water amount of up to 95% in many cases. Hydrogels can be obtained from either natural (*e.g.*, hyaluronic acid, chitosan, gelatin, polypeptides and polysaccharides) or synthetic polymers (*e.g.*, poly(vinyl alcohol), poly(ethylene glycol) and poly(acrylamide)).[20, 21] Among the most used polymers for hydrogel fabrication, hyaluronic acid (HA) has attracted a high interest over the years because of its distinctive biological properties. Indeed, these hydrogels exhibit features very close to those found in human tissues.[22, 23] HA is a biocompatible and anionic mucopolysaccharide that can be extracted from mammalian connective tissue, extra-cellular matrix (ECM) and synovial fluid of vertebrates. It is already used for cosmetic, biomedical and tissue engineering applications.[22, 23] HA hydrogels can be obtained from simple chemical cross-linking using divinylsulfone (DVS) or 1,4-butanediol diglycidyl ether (BDDE) under alkaline conditions.[24, 25] Poly(allylamine), denoted as PAH, is a water-soluble, biodegradable and cationic polyelectrolyte with pendant primary amino groups. To date, studies on PAH-based hydrogels have been surprisingly rare, even though they exhibit interesting adhesive and antimicrobial properties in applications in the biomedical field.[26-28] PAH hydrogels can be obtained from chemical cross-linking using glutaraldehyde or epichlorohydrin under acidic conditions.[29] Despite their respective interesting properties, few associations of HA and PAH especially towards multilayer films or hydrogels have been reported in the literature. As HA and

PAH exhibit opposite charge, they can be associated according to the LbL process to produce multilayered hydrogels.[30] Previous works highlighted that these materials in the absence of any chemical crosslinking are highly sensitive to pH and ionic strength.[31, 32] The authors of these works evidenced that the swelling ratio of this type of hydrogel is related to the total number of layers and the pH of the assembly solution.[31, 33] They also suggested that the swelling behavior of PAH-HA hydrogels can be tuned by controlling the ionic strength and thus allowing interesting applications and especially for the controlled release of active drugs, membrane filtration, and biomaterial coatings.[33-35] Investigating the mechanical properties can provide insight into intermolecular interactions in the materials and is thus of fundamental interest.[36] However, mechanical measurements on PEMs and hydrogels can be complex and experimentally challenging, especially when the thickness of these materials is of a few micrometers.[37] Macroscopic mechanical measurements on thin materials (few hundred nm) often fail and the use of atomic force microscopy (AFM) in force spectroscopy mode is required. Indeed, many techniques using AFM has been developed to address the mechanical properties of thin and soft materials providing local and spatially resolved information.

Infrared spectroscopy in attenuated total reflection mode (ATR-FTIR) is a useful complementary method to obtain information on the chemical composition of multilayer films *in situ*.[38-40] However, analysis of infrared spectra is not always clear because of their complexity and often weak spectral changes. To help the analysis of these experimental data, a computational statistical method is useful. Here, a chemometric method was used that allows estimation of the spectra of pure components from the whole vibrational spectra recorded. The Bayesian positive source separation (BPSS) curve resolution method[41-43] was chosen for analysis and interpretation of the experimental data. BPSS gives an estimation of the pure component spectra and the relative concentrations of the underlying compounds.[44-46]

In the present work, several PAH-HA based hydrogels built according to the LbL method were chemically cross-linked using either BDDE or DVS to target preferentially primary alcohol groups of HA and possibly amine groups of PAH. Time evolution of both mechanical features and chemical structure of the hydrogels during their cross-linking were addressed by combining infrared spectroscopy, AFM and force spectroscopy. Statistical analysis of the infrared spectra based on the Bayesian Positive Source Separation method (BPSS) allows deciphering hydrogel's chemical structure and their possible description into a linear combination of pure HA and PAH hydrogels.

Materials and methods

Chemicals.

Tris(hydroxymethyl)aminomethane (TRIS, ref. T4661), sodium chloride (NaCl, ref. 1.06406.0500), sodium hydroxide (NaOH, ref. S5881-1KG), 1,4-Butanediol diglycidyl ether (BDDE, ref. 220892), N-(3-Dimethylaminopropyl)-N′-ethylcarbodiimide (EDC, ref. E7750-5G), divinyl sulfone (DVS, ref. 8212150010) and N-hydroxysuccinimide (NHS, ref. 130672-5G) were purchased from Sigma-Aldrich (France) and poly(allylamine hydrochloride) (PAH, Mw = 50,000 g/mol, ref. 283223) was purchased from Polysciences (Biovalley, France). Sodium hyaluronate (HA, 301- 450 kDa, ref. HA500K-1) was purchased from LifeCore Biomedical (Chaska, USA). Structures and characteristics of the polymers and the cross-linking agents are reported in Supplementary Information (**Table S1**)

Preparation of HA-BDDE, PAH-BDDE, HA-DVS and PAH-DVS hydrogels.

HA-BDDE, PAH-BDDE, HA-DVS and PAH-DVS hydrogels were obtained from an equivolume mixing of polymers and the cross-linking agents according to the following procedure. HA and PAH were diluted to final concentrations at 50 mg/mL in NaOH 1% by vortex stirring for 10 minutes at room temperature. Cross-linking agent, *i.e.*, BDDE at 500, 1000 or 1500 mM, or DVS at 50, 100, 250, 500 or 1000 mM final concentrations in NaOH 1%, was added to HA or PAH solutions. Then the mixture was deposited onto a borosilicate glass disk (Preciver, France) of 14 mm diameter into a well and stirred at 200 rpm, at room temperature for 24 h or 2 h, respectively. After gelation, samples were rinsed 3 times for 10 minutes in a solution of NaCl 150 mM, TRIS 10 mM at pH 7.4 prior to store it at 4°C in this buffer solution until further analysis. Cross-linking agents concentration were selected in a broad range from conventional concentrations used in biomedical applications to large excess to reach the saturation of all reactive sites.

Preparation of $(PAH\text{-}HA)_{30}$ based hydrogels.

$(PAH\text{-}HA)_{30}$ based hydrogels were obtained according to the layer-by-layer (LbL) method using a dipping robot (Riegler & Kirstein GmbH, Berlin, Germany). For the AFM measurements, the PEM were prepared onto borosilicate glass disk of 14 mm diameter and 0.95 mm thick (Preciver, France). For the infrared measurements, the PEM were directly formed onto a Ge crystal enclosed in a batch cell. The first deposited layer consisted of PAH at 1 g/L in the (NaCl, TRIS) buffer solution during 5 minutes, and then the sample was rinsed by immersion for 5 min in the (NaCl, TRIS) buffer solution at pH 7.4 consisting of NaCl at 150 mM and TRIS at 10 mM. The second deposited layer consisting of HA at 1 g/L in the (NaCl, TRIS) buffer solution during 5 minutes was subsequently applied with following the procedure described above for the deposition of the PAH layer. The hydrogel build-up process was iterated via an alternate deposition of the polycationic and of the polyanionic polymers until it consisted of 30 bilayers.

At the end of the build-up process, the $(PAH\text{-}HA)_{30}$ based hydrogels were cross-linked by overnight immersion either into a solution of BDDE at 5, 50, 250, 500, 1000 or 1500 mM in (NaCl, TRIS) buffer at pH 10, or into a solution of DVS at 10, 50, 100, 250, 500 or 1000 mM in (NaCl, TRIS) buffer at pH 10. After the chemical cross-linking with BDDE or DVS, all samples were extensively rinsed 3 times for 20 minutes in a bath of (NaCl, TRIS) buffer at pH 7.4 and then stored in the same buffer at 4°C prior to AFM and IR experiments. The build-up of the $(PAH\text{-}HA)_{30}$ based hydrogels and its cross-linking procedures are summarized in **Scheme 1 (see supporting information)**. Reference samples have been prepared by cross-linking of native $(PAH\text{-}HA)_{30}$ based hydrogels using several solutions of EDC at 6.4, 9.6, 16, 25, 50, 100, 250, 500 or 1000 mM in (NaCl, TRIS) buffer supplemented with NHS 10 mM at pH 5.5. After chemical cross-linking, all reference samples were extensively rinsed 3 times for 20 minutes in a bath of (NaCl, TRIS) buffer at pH 7.4 and then stored in the same buffer at 4°C for further experiments.

Atomic force microscopy.

AFM images and force spectroscopy measurements were performed using a Bioscope Resolve (Bruker Nano Surface, Bruker France SAS, Palaiseau, France) and a MFP3D-BIO instrument (Asylum Research Technology, Oxford Instruments Company, Wiesbaden, Germany), respectively. The topography of the PEM films was imaged by AFM operating in contact mode. Silicon nitride cantilevers of conical shape purchased from Bruker (MLCT, Bruker France SAS, Palaiseau, France) with a spring constant of about 9-14 pN/nm were used for both imaging and

PEM nanomechanical measurements. All images were recorded with a resolution of 512 × 512 pixels and a scan rate of 1 Hz. Nanomechanical properties of the PEM films were addressed in PBS buffer solution (pH 7.4) by recording 4 Force-Volume Images (FVI) at 4 different locations of the films (4128 measurements per condition). Each FVI consisted of a grid of 32 × 32 force curves measured with adopting a 2 μm.s^{-1} approach rate of the tip toward the sample. The Young modulus E was evaluated by analysing the force-indentation curves within the framework of the Sneddon model.[47, 48] In this model, the Young modulus is related to the applied force according to the equation given below:

$$F = \frac{2E \cdot \mathrm{Tan}(\alpha)}{\pi(1-\nu^2)} R^{1/2} \delta^2 \cdot f_{\mathrm{BECC}}$$

where δ is the indentation depth, ν the Poisson coefficient, α the semi-top angle of the conical tip and f_{BECC} is the bottom effect cone-correction function that takes into account the stiffness of the glass substrate that supports the PEM material. All FVI were analysed using an automatic Matlab algorithm detailed elsewhere,[49] and the average Young moduli values given in this work were derived from at least 3072 force curves.

Infrared Spectroscopy.

The attenuated total reflectance Fourier transform infrared (ATR-FTIR) spectra were recorded between 4000 and 700 cm^{-1} on a Vertex 70v spectrometer (Bruker, Karlsruhe, Germany) equipped with a KBr beam splitter and a deuterated triglycine sulphate (DTGS) thermal detector. The resolution of the single beam spectra was 4 cm^{-1}. All interferograms were Fourier processed using the Mertz phase correction mode and a Blackman-Harris three-term apodization function. No ATR correction was performed. ATR spectra are shown with an absorbance scale corresponding to

$\log(R_{reference}/R_{sample})$, where R is the internal reflectance of the device. A SPECAC home-modified ATR-FTIR batch cell enclosing a trapezoidal Ge crystal (72 mm x 10 mm x 6 mm, refraction index: 4.0) with an incidence angle of 45° yielding six internal reflections on the upper face in contact with the sample was used. The spectra were recorded at 21 ± 1°C in an air-conditioned room. Recording of spectra, data storage and data processing were performed using the Bruker OPUS 7.8. Each experiment presented here is representative of two independently conducted measurements. The spectral evolution was monitored for 2 h up to 24 h depending on the experiment (200 scans, spectra recorded every 3 minutes, 30 minutes or one hour depending on the time-progress of the experiment). The water vapor was subtracted and the baseline was corrected (points at: 3585, 2750, 1800, and 900 cm^{-1}), before integrating the chosen peak intensities. Calibration curves were obtained for HA, PAH, BDDE and DVS by recording spectra of these compounds at 5 increasing concentrations. These curves allowed obtaining estimated concentrations of the different compounds in the vicinity of the ATR crystal (**Table S3**).

Spectral curve resolution analysis with the Bayesian Positive Source Separation method.

The resolution of the pure component spectra from the “mixture” infrared spectra information was performed with a statistical method of spectral mixture analysis called BPSS, for Bayesian Positive Source Separation.[42, 43] Singular value decomposition (SVD) was used to estimate the rank of the data sets. The usual approximation is that the number of large singular values, significantly different in magnitude from the noise related singular values, indicates the rank of the analyzed matrix. In principle, a successful separation can be achieved by using the appropriate number of components. An advantage of BPSS is that the number of components can be introduced into the algorithm and several trials can be conducted within minutes until the error matrix does not carry recognizable spectral features. Thus, the number of components may be chosen from SVD, but it is ultimately the algorithm that shows whether the number of requested components is correct. The lack of fit is used to assess how the estimated pure component spectra and mixing coefficients can reproduce the observed data. By assuming a known number of components, the mixture analysis aim is to estimate the pure component spectra and the mixing coefficient profiles from the mixture spectra. Without any calibration reference, it is possible to obtain relative concentrations by using BPSS and a mass-balance constraint.[41] It must be emphasized that these concentrations are relative since they are weighted by the intensity of the normalized pure component spectra and not by a separate calibration. The analyses were performed in spectral region 1800-800 cm^{-1} of baseline corrected spectra. IR-ATR spectra were recorded as a function of time on each sample from each chemical treatment. Between 60 up to 140 spectra were analyzed for each series of spectra. Spectral sources were estimated, and their mixing coefficients are presented as a function of time. Where useful, calculations were performed with imposed sources as constraints. When applicable, the constraints are specified in the figure captions. Non reconstructed data were mainly noise, and represented by less than 10% of all results.

Results and discussion

Evolution of spectral fingerprint of $(PAH\text{-}HA)_{30}$ based hydrogel during its cross-linking.

(PAH-HA) hydrogels consisting of 30 bilayers were built-up according to LbL method with solutions of PAH and HA at 1 g/L or 2 μM, and then subsequently cross-linked with BDDE or DVS at several concentrations (from 5 mM to 1500 mM in basic conditions) as briefly described in Supporting Information (**Scheme 1**). The hydrogel build-up and its subsequent cross-linking was monitored by ATR-FTIR, through the recording of spectra after each layer deposition (**Figure**

1). During the build-up step the intensity of the overall spectra are increasing as a function of the number of bilayers indicating the deposition of the polymers (**Figure 1a**). The main band assignments were performed according to the literature[50-52] and are gathered in **Table S2**). Three main spectral regions can be distinguished:

- Between 1800 and 1500 cm^{-1}, bands at 1645, 1600, 1540, and 1525 cm^{-1} are assigned to amide I band, $\nu_a COO^-$, amide II band from HA, and $\delta_a NH_3^+$ from PAH, respectively.
- Between 1500 and 1200 cm^{-1} bands at 1457, 1415 and 1378 cm^{-1} are assigned to δ CH_2, from PAH, $\nu_s COO$ δCH_3 from HA, respectively.
- Between 1200 and 800 cm^{-1}, the overlapped bands were assigned to C-C C-O-C, C-O-H stretching's from glycosidic rings.

The analysis of the infrared spectra collected during the film build-up was carried out using the BPSS chemometric method. A good reconstruction of these spectra is obtained using two sources, which are similar to the spectra of pure HA and PAH (comparison in **Figure S1a**). The mixing coefficients of the two extracted sources are presented in **Figure S1b** as a function of the numbers of bilayers. The ratio of both mixing coefficients decreases from 0.87 to 0.50 ± 0.02 reaching a pseudo-plateau from 12 bilayers (**Figure S1**). The penetration depth of the evanescent wave was calculated at 0.6 µm at 1100 cm^{-1} with a refractive index of 1.5 for the bilayers. The calculated ratios suggested that from 12 bilayers the coverage of the surface was homogeneous and the thickness of the film was above 0.6 µm. From 12 bilayers, there is effective coalescence of the deposits of the polymer's islands present.[53, 54] The chemometric analysis revealed that the concentration of each polyelectrolyte within the film increased during the build-up from 2 and 20 µM for HA and PAH (1 g/L) up to 700 and 300 µM (*i.e*. 315 g/L for HA and 15 g/L for PAH).

After construction, the resulting $(PAH\text{-}HA)_{30}$ based hydrogel was exposed either to BDDE or DVS solutions in order to cross-link it through bridges between OH groups of the HA chains according to reactions reported in the literature[55] **(Figure S2)**, i.e., these reactions should occur mainly in the HA enriched layers/areas of the hydrogel. Yet, it was reported that both BDDE and DVS can react with NH_2 groups of PAH[56] leading also to the cross-linking in the PAH enriched layers/areas of the hydrogel (**Figure S3)**.

Chemical changes occurring with $(PAH/HA)_{30}$ based hydrogels during their cross-linking, either with a solution of BDDE at 500 mM or DVS solution at 250 mM were monitored for 24 h using the spectrum of the $(PAH/HA)_{30}$ film before exposure to the cross-linker as the reference. In this way, all positive and negative bands are a result of the modifications within $(PAH\text{-}HA)_{30}$ based hydrogels. **Figure 1b** shows the time-evolution of the spectra during the exposure of $(PAH/HA)_{30}$ to BDDE. Negative bands with the general feature of $(PAH/HA)_{30}$ are observed (**Figure 1a-b**). Positive bands with increasing intensities also occur at 1250, 1109 and 908 cm^{-1}. The bands at 1250 and 908 cm^{-1} are assigned to the antisymmetric and symmetric respiration of the epoxy ring from BDDE, respectively. The band at 1109 cm^{-1} is assigned to antisymmetric stretching of the C-O-C bond of ethers.[57] Altogether these results indicated a significant loss or upward-diffusion of HA and PAH near the Ge crystal surface whereas the increase of the band assigned to epoxy groups of BDDE indicated the diffusion of unreacted BDDE from the surface to the bottom of the $(PAH\text{-}HA)_{30}$ based hydrogel. Furthermore, the increase of ether bands shows the reaction of alcohols functions with the BDDE epoxy cycle and consequently the cross-linking between HA chains with possible lateral branching.[58] The decrease in HA concentration within the film strongly suggest the occurrence of free or mobile HA chains and their release when they have not been cross-linked even if cross-linkers concentrations were in excess.

Figure 1c shows the spectral time-evolution of a $(PAH\text{-}HA)_{30}$ based hydrogel during the exposure to DVS. The spectral modifications are very different than those observed during the exposure of the $(PAH\text{-}HA)_{30}$ based hydrogel exposed to BDDE. Indeed, decreases of the intensities in region 1700-1400 cm^{-1} are observed and they are about 5 times lower than those measured with BDDE, suggesting a much lower loss or upward-diffusion of HA and PAH near the Ge surface. Besides, increasing bands at 1300 and 1130 cm^{-1} are observed, and they are associated to the stretching vibrations of sulfone groups in DVS (**Table S2**). The slight decrease of the wavenumbers with respect to free DVS suggest the reaction of DVS with the $(PAH\text{-}HA)_{30}$ based hydrogel. Furthermore, the increase of a band at 1190 cm^{-1} is observed as a function of time. It is assigned to C-N-C stretching typical for secondary amines and was not observed in the spectra in **Figure 1b**.[57] The spectra did not clearly show bands associated with ether bonds between 1140 and 1085 cm^{-1} even on second derivative spectra (data not shown). This result indicates that the reaction of DVS with the $(PAH\text{-}HA)_{30}$ based hydrogel mainly occurs with the primary amine bonds from PAH.

To monitor the evolution of HA, PAH, BDDE and DVS amounts during the cross-linking reactions, we performed a BPSS analysis with the infrared spectra of $(PAH\text{-}HA)_{30}$ based hydrogel recorded for 24 hours during its exposure to BDDE or DVS. **Figures 2a,b** show the extracted sources in both series of spectra. The estimated spectra were typical for HA, PAH and BDDE or HA, PAH and DVS. The corresponding time-evolution of the sources are presented in **Figure 2c,d**. An exponential increase of BDDE concomitant to an exponential decrease of the HA and PAH mixing coefficients are observed over 24 hours. A plateau is reached after 8 hours (**Figure 2c**). These results evidenced that both HA and PAH have been modified by exposure to BDDE. For the PAH polyelectrolyte, the mixing coefficient reached the zero value. In the close vicinity above the crystal (~ 1 µm), no native PAH was observed from 10 h of exposure to BDDE. In contrast, the HA mixing coefficients stayed at about 24% after 8 hours. This means that HA only partially reacted. The time-evolution of the mixing coefficients were fitted according to the following exponential decay model:

$$C(t) = C_0 + C_1 e^{-\frac{t}{t^*}}$$

where $C_0 + C_1$ is the maximal mixing coefficient, C_0 the final mixing coefficient and t^* the time constant. Then, the reaction rate k can be calculated according to the following equation:

$$k = \frac{1}{t^*}$$

From these results, we calculated a reaction rate of 0.32 h^{-1} and 0.24 h^{-1} for HA and PAH, respectively (**Table 1**). The discrepancy between BDDE reactivity regarding HA and PAH showed that the reaction kinetics of BDDE with HA is 1.3 times higher than with PAH. However, HA was only partially chemically modified, whereas the contribution of native PAH was canceled after ~ 10 hours. This result suggests that BDDE affinity or reactivity for primary alcohol groups (from HA) is lower than for primary amine groups (from PAH).

Figure 2d shows the time-evolution data obtained when $(PAH\text{-}HA)_{30}$ based hydrogel was exposed to DVS. An exponential increase of DVS concomitant to an exponential decrease of the HA and PAH mixing coefficients are observed over 24 hours. A pseudo-plateau is reached in 2 hours. After 30 minutes, the PAH mixing coefficient was 0, whereas the HA mixing coefficient continued to decrease to 20% until 6 hours of DVS exposure. The calculated reaction rates k were of 0.44 h^{-1} and 5.21 h^{-1} for HA and PAH, respectively (**Table 1**). The DVS affinity or reactivity is more than 11 times higher for primary amine groups (from PAH) than for primary alcohol groups (from HA). Altogether, infrared measurements indicated that major structure modifications occurred within $(PAH\text{-}HA)_{30}$ based hydrogels during their cross-linking with BDDE or DVS. Such molecular modifications should significantly impact on their morphology and mechanical properties. To address this hypothesis, atomic force microscopy is a relevant tool to decipher morphological features (thickness and roughness) as well as mechanical ones (stiffness and swelling ratio) of $(PAH\text{-}HA)_{30}$ based hydrogels upon chemical cross-linking with BDDE and DVS at several concentrations.

Morphology and mechanical evolution of $(PAH\text{-}HA)_{30}$ based hydrogels under BDDE and DVS exposure.

AFM images were recorded for $(PAH\text{-}HA)_{30}$ based hydrogels previously chemically cross-linked by BDDE or DVS at different concentrations, to highlight possible changes in morphology due to chemical cross-linking, and relate them with the structural modifications described above. As illustrated in **Figure 3**, no significant surface modifications have been observed whatever the cross-linker used, but film roughness is increased with BDDE concentration during cross-linking from *ca.* 7 nm up to 23 nm (**Table 2**). Concerning cross-linking with DVS, the impact on roughness is tenuous with values in the range of 6-10 nm whatever the DVS concentration considered (**Table 2**). Conversely, the analysis of the thickness after cross-linking evidenced an important contraction of the native $(PAH\text{-}HA)_{30}$ based hydrogel depending on the BDDE concentration. Indeed, the thickness loss was approximately a factor of 1.2 to 1.5 when $(PAH\text{-}HA)_{30}$ based hydrogels were exposed to BDDE concentrations of 5 to 1500 mM. No thickness modifications were observed when the $(PAH\text{-}HA)_{30}$ based hydrogels were cross-linked with DVS and the values remained at about 4.6 µm whatever the considered concentration (**Table 2**).

We have further studied, and systematically compared, the evolution of the elasticity of hydrogels cross-linked by BDDE or DVS, with the data obtained for cross-linking using the classical method with 1-ethyl-3-(3-dimethylaminopropyl)carbodiimide (EDC), as reported in **Figure 4a**. EDC is a cross-linking reagent that creates direct covalent bonds between primary amines and carboxylic groups through nucleophilic substitution.[59, 60] Several works concerning the crosslinking of hyaluronic acid based-hydrogels, reported that mechanical properties, *i.e.* stiffness can be tuned with EDC concentration with values ranging from a few kPa up to 500 kPa for hydrogels based on association of poly(L-lysine) (PLL) and HA.[34, 39, 61] All mechanical measurements were performed by AFM using the nanoindentation technique on fresh samples. In line with infrared results, the stiffness of $(PAH\text{-}HA)_{30}$ based hydrogels was strongly impacted by the chemical cross-linking with a resulting elasticity that increased with the concentration of cross-linker. Whatever the cross-linker molecule, it leveled off at high enough concentrations before reaching a plateau value. Overall, this increase in stiffness amounted to *ca.* 7 kPa up to 150, 250 and 800 kPa for maximal concentration in BDDE, DVS and EDC, respectively. Such qualitative dependence of material stiffness on chemical cross-linking has been already extensively reported for polyelectrolyte multilayer-based hydrogels and other polymer-based hydrogels cross-linked with EDC that is commonly used as a reference molecule for hydrogels stiffening.[12, 59] It can be highlighted that $(PAH\text{-}HA)_{30}$ based hydrogels cross-linked with DVS are systematically and almost twice stiffer than those cross-linked with BDDE whatever the considered concentration. This discrepancy should come from a difference in chemical reactivity, as observed by the infrared analyses, as well as by the size/flexibility of the bridges created between the HA chains during the cross-linking reactions (**Scheme 2** in Supporting Information). Shorter and less flexible bridges generated by DVS molecules should lead to shorter mesh size from the HA chains network and then a stiffer material (*e.g.*, DVS bridges are about 0.96 nm against 1.98 nm for BDDE ones). However, $(PAH\text{-}HA)_{30}$ based hydrogels cross-linked with BDDE and DVS remained systematically 4 to 5 times softer than those cross-linked with EDC for the same concentration. Such differences should be due to the fact that HA and PAH are intimately connected to each other by EDC according to amide bonds conversely to DVS and BDDE that mainly interconnected HA and PAH chains to each other through side bridging (**Figures S2** and **S3)**. Surprisingly, the swelling ratio of $(PAH\text{-}HA)_{30}$ based hydrogels according to the cross-linking procedure reported in **Figure 4b** and **Table 2** evidenced a very similar dependence between the swelling ratio and the stiffness whatever the cross-linker molecule used. Indeed, this ratio decreased from about 8-9 for native films down to 2 for highly cross-linked ones (**Figures S4 and S5**).

The peculiar mechanical behavior of $(PAH\text{-}HA)_{30}$ based hydrogels upon cross-linking with either BDDE or DVS should also be driven by the degree of HA and PAH connections through the cross-linker bridges between the polymer chains. Such assumption is motivated by the layer-by-layer organization or structure of $(PAH\text{-}HA)_{30}$ based hydrogels that contain overlaid and enriched layers of HA and PAH. Chemical cross-linking of such multilayered hydrogels should lead to the formation of layers enriched in only cross-linked HA chains, enriched in only cross-linked PAH chains and mixed layers at the interface of previous ones containing HA and PAH chains linked together by BDDE or DVS. To address this assumption and attempt to quantify the mechanical contribution of cross-linked HA chains denoted as HA-BDDE and HA-DVS and of cross-linked PAH chains denoted as PAH-BDDE and PAH-DVS, we decided to determine the mechanical properties of pure HA and PAH hydrogel using nanoindentation technique by AFM for several BDDE and DVS concentrations (**Table 3** and **Figure S6)**. Our results evidenced that HA hydrogels exhibited low stiffness when BDDE was used as cross-linking agent (from 0.6 to 3.4 kPa depending on BDDE concentration), whereas DVS cross-linking led to hydrogels 30 up to 100 times stiffer (from 106 to 151 kPa) with respect to HA-BDDE hydrogels. The mechanical features of PAH hydrogels were different according to a given concentration in cross-linking agents. Indeed, those obtained from BDDE cross-linking reaction (in the range of 179 up to 238 kPa) were 2 up to 3 times softer than those obtained from DVS cross-linking reaction at the same concentration (*i.e*. in the range of 384 up to 730 kPa). As the cross-linking of $(PAH\text{-}HA)_{30}$ based hydrogels led to mechanical properties in the range of 51 up to 79 kPa with BDDE at the same concentrations and values in the range of 103 up to 174 kPa with DVS, HA mechanical contribution appeared obviously weaker than the one of PAH. Besides, the maximal stiffness of $(PAH\text{-}HA)_{30}$ based hydrogels cross-linked either by BDDE or DVS was systematically lower than values measured for PAH-BDDE and PAH-DVS hydrogels for the same cross-linking agent concentration. This mechanical behavior can be due to the huge amount of HA within the $(PAH\text{-}HA)_{30}$ based hydrogels that was twice the concentration of PAH.

Spectral evolution of pure HA and PAH hydrogels during their formation

HA hydrogels denoted as HA-BDDE and HA-DVS were obtained after mixing a pure solution of HA at 0.2 mM with either BDDE or DVS in alkaline conditions at 1000 mM and 250 mM, respectively. The infrared spectra of HA, BDDE and DVS are progressively modified over the 24 h of the *in situ* monitoring (**Figures 5a** and **5b)**. When HA was exposed to BDDE, the recorded spectra have the general feature of BDDE and its products after reaction with HA and/or water. These results indicated the significant loss of HA and a progressive and huge accumulation of BDDE within HA-BDDE hydrogels split into free/unreacted molecules, coupling and lateral branching or pending BDDE (**Figure S2)**. The shape of the most intense bands absorbing between 1200 and 1000 cm^{-1}, assigned to νC-O-C, νC-OH, νC-C, νC-O-C from BDDE and HA (**Table S2**), changed over time. The initial bands were gradually replaced by new bands at 1131, 1110, 1086 and 1040 cm^{-1}. In parallel, two bands at 1257 and 908 cm^{-1} decreased. These two bands are assigned to the antisymmetric and symmetric stretching bands of the BDDE epoxy group. They show the opening of the epoxy group upon reaction with HA. If one cannot exclude hydrolysis reactions with water, the observed bands in region 1200-1000 cm^{-1} cannot be assigned to water hydrolysis because bands absorbed in this case at 1109, 1095 and 1073 cm^{-1} (data not shown). Such results indicated that the epoxy rings of BDDE are progressively opened while ether bonds are formed between BDDE and primary alcohol groups of HA.

When HA was exposed to DVS, the evolution of the spectra was observed for only 120 minutes. Then the spectra did not evolve significantly. The region above 1500 cm^{-1} did not change significantly, the reaction of HA with DVS did not imply the carboxylate moiety of HA. In the region between 1350 and 1200 cm^{-1}, a new band appeared at 1317 cm^{-1}, it may be assigned to C-O stretching of the new band created by the reaction of DVS with one alcohol of the sugar ring (**Figure S3**). The evolution of the spectra as a function of time shows also the shifts of the bands initially at 1300 and 1251 cm^{-1} to 1287 and a shoulder at 1265 cm^{-1}, respectively. These bands are assigned to νaSO_2 and δCH from DVS, respectively. This downshift shows the increase of the molecular weight around the corresponding bonds, and therefore the reaction of DVS with HA. Moreover, the νsSO_2 band from DVS, absorbed at the begining of the monitoring at 1129 cm^{-1} (**Table S2)**, was downshifted and splitted into two bands at 1124 and 1116 cm^{-1}. This feature can be assigned to two different environments around the sulfone bond consistent with a difference in binding mode (pending or coupling reactions) (**Figure S3**). The spectral evolution of HA-DVS was faster than with BDDE, and the gelation occurred in a few minutes without significant modification of the initial amount of HA in close contact with the ATR Ge crystal. Infrared observations evidenced a huge accumulation of DVS overtime and the decrease of in-plane/out-of-plane CH deformation bands associated with the loss of ethylenic double bond at 987 cm^{-1}.

The ATR-FTIR of PAH exposed to DVS or BDDE were monitored *in situ* over 24 h according to the protocol also used for HA hydrogels. (**Figures 5c** and **5d)**. The spectra show the decrease of bands at ~1515 cm^{-1} assigned to δNH_3^+ from PAH. Bands at 1257 and 907 cm^{-1}, assigned to the stretching vibrations of the epoxy groups decreased as a function of time (**Figure 5c**). In parallel, bands at 1126, 1113 appeared. They are assigned to C-O, C-O-C stretching bonds of new compounds originating from the reaction of BDDE with PAH. These results show that BDDE was reacting with PAH. **Figure 5d** relates to the infrared monitoring of PAH exposed to DVS. Spectral evolution evidenced a quasi-instantaneous reaction between PAH and DVS when they are mixed. Indeed, no significant bands decrease within the infrared spectra was noticed but only important increases of the bands intensities at 957, 986, 997, 1127, 1183, 1251, 1300, 1390, 1450 and 1463 cm^{-1}. Most of these bands have been assigned to DVS, as reported in **Table S2**.

Kinetic monitoring of the biochemical fingerprint of each hydrogel obtained from cross-linking with BDDE and DVS was followed to address the chemical partition of cross-linked HA and PAH within $(PAH\text{-}HA)_{30}$ based hydrogels according to their cross-linking with BDDE and DVS. **Figure 6a** shows the time evolution of native BDDE during the formation of HA-BDDE and PAH-BDDE hydrogels, respectively. Our measurements evidenced an exponential decrease of the unreacted BDDE concentration over 24 h for both HA-BDDE and PAH-BDDE hydrogels. However, no plateau value was reached over this period for both hydrogels, suggesting that cross-linking reaction was not finished. By fitting these data according to an exponential decay model as previously recorded, we calculated constant times and reaction rates as reported in **Table 1**. Constant times of 13.2 h and 26.7 h were calculated during the formation of HA-BDDE and PAH-

BDDE hydrogels, respectively. These results evidenced that BDDE cross-linking reaction is twice faster with HA than with PAH. **Figure 6a** clearly suggests a greater affinity of BDDE to react with primary -OH groups of HA than -NH_2 groups of PAH as documented in the literature.[62, 63] One can emphasize that cross-linking reaction of HA or PAH alone with BDDE is 4 times slower than the same reaction when both polymers are mixed within the $(PAH\text{-}HA)_{30}$ based hydrogels. Similar behavior has evidenced a 6 times slower crosslinking reaction with DVS. **Figure 6b** shows the time evolution of unreacted DVS during the formation of HA-DVS and PAH-DVS hydrogels. The reactivity of DVS was higher with respect to BDDE cross-linker and the chemical reaction was faster. Indeed, the gelation of HA and PAH solutions occurred in a few minutes (also observed by the eyes) and the plateau value of DVS exponential decay was reached in less than 30 minutes. Constant times of 0.21 h and 0.02 h were calculated for HA-DVS and PAH-DVS hydrogels, respectively. These results clearly evidenced that the affinity or reactivity of DVS with primary amine is 10 times higher than with primary alcohol of HA. Besides, the cross-linking reaction of HA or PAH alone with DVS was 10 times slower than the same reaction when both polymers are mixed within the $(PAH\text{-}HA)_{30}$ based hydrogels.

Altogether, these results clearly indicated that the cross-linking efficiency and the reactivity of BDDE or DVS towards pure HA or PAH were very different. Besides, the reaction kinetic parameter (*i.e.*, constant time or reaction rate) was very different when the two polymers were mixed according to layer-by-layer construction used for $(PAH\text{-}HA)_{30}$ based hydrogels. These modifications may be also related to the competition between the primary alcohol and amine sites towards the epoxy groups of BDDE and the ethylenic bonds in the case of DVS. Such competition may impact the structure of cross-linked $(PAH\text{-}HA)_{30}$ based hydrogels as they were built-up according layer by layer procedure. Indeed, this peculiar layer by layer construction of (PAH-

HA)$_{30}$ based hydrogels may lead to the superposition of enriched layers containing only cross-linked HA chains (*i.e.*, HA-BDDE or HA-DVS), enriched layers containing only cross-linked PAH chains (*i.e.*, PAH-BDDE or PAH-DVS) and mixed layers at the interface of previous ones containing HA and PAH chains linked together by BDDE or DVS. Bayesian Positive Source Separation (BPSS) chemometric procedure is a relevant method to address this hypothesis and estimate the partition or mixing coefficients of cross-linked (PAH-HA)$_{30}$ based hydrogels into pure HA and PAH hydrogels combination.

Structural and mechanical correlation between HA and PAH pure hydrogels and cross-linked (PAH-HA)$_{30}$ based hydrogels.

We have performed a BPSS analysis with spectral constrains consisting in infrared data of initial (PAH-HA)$_{30}$ based hydrogel, and final HA-BDDE, PAH-BDDE, HA-DVS and PAH-DVS hydrogels. The time-evolution of the mixing coefficients calculated from the ATR-FTIR spectra recorded during the cross linking of (PAH-HA)$_{30}$ based hydrogel either with BDDE or DVS are presented in **Figure 7**. This constrained analysis evidenced that the linear combination of infrared signatures of final HA gels (with BDDE or DVS cross linkers), PAH gels (with BDDE or DVS cross linkers) and native (PAH-HA)$_{30}$ based hydrogels allowed to explain ~90% of the infrared fingerprint evolution during the crosslinking of (PAH-HA)$_{30}$ based hydrogels with BDDE and DVS. **Figure 7a** shows the time evolution of the mixing coefficients during the crosslinking of (PAH-HA)$_{30}$ based hydrogels with BDDE derived from the constrained BPSS estimation. Our results evidenced that the spectral contribution of native (PAH-HA)$_{30}$ based hydrogels within the global infrared fingerprint decreased exponentially with time during the cross-linking reaction and the contribution of native (PAH-HA)$_{30}$ based hydrogels in the spectra was reduced to 4% after 10

h. Concomitantly, the spectral contribution of PAH-BDDE and HA-BDDE hydrogels increased exponentially until rising to a maximal plateau after 8 h with values of 16% and 80%, respectively. This analysis allowed assuming that the final molecular structure of $(PAH\text{-}HA)_{30}$ based hydrogels after 24 h cross-linking reaction with BDDE was close or similar to the one of HA-BDDE and PAH-BDDE hydrogels with partition of 16 and 80%, respectively. It can be highlighted that the discrepancy between the two mixing coefficients could be mediated by the affinity of BDDE to react with primary –OH and $–NH_2$ functional groups as well as by their concentration within the $(PAH\text{-}HA)_{30}$ based hydrogels. However, the careful inspection of mechanical analyses performed on $(PAH\text{-}HA)_{30}$ cross-linked by BDDE as reported in **Table 3** and **Figure S6** revealed that the latter is softer than the pure PAH-BDDE hydrogel. This means that PAH-BDDE mechanical contribution is lower than the one of HA-BDDE in line with the mixing coefficient determined from chemometric analyses illustrated in **Figure 7a**. Here, the mechanical feature of $(PAH\text{-}HA)_{30}$ cross-linked by BDDE can be described as a linear mechanical combination of HA-BDDE and PAH-BDDE hydrogels with partition of about 67% and 33% respectively. We emphasize that the mechanical contribution of HA-BDDE appeared slightly lower than the chemical ones. Such discrepancy between mechanical and chemical features could be explained by the presence of much more pending BDDE on the HA chains than PAH ones as expected in the PEM as illustrated by **Figure S2**. Indeed, the mechanical contribution of pending BDDE to polyelectrolytes network should be negligible as compared to the one of coupling BDDE.

Concerning the structure of $(PAH\text{-}HA)_{30}$ based hydrogels after cross-linking with DVS, the spectral contribution of native $(PAH\text{-}HA)_{30}$ based hydrogels within the global infrared fingerprint also decreased exponentially with time and was totally canceled after 1 h, whereas 8 h was required to observe an equivalent decrease with the BDDE cross linker. Concomitantly, spectral contribution of PAH-DVS and HA-DVS hydrogels increased exponentially until rising to a maximal plateau after 1 h with values of 45% and 55%, respectively. It can be assumed that the final molecular structure of $(PAH\text{-}HA)_{30}$ based hydrogels after 24 h cross-linking reaction with DVS was similar to the one of PAH-DVS and HA-DVS hydrogels with the partition of 45 and 55%, respectively. Here, that discrepancy between the two mixing coefficients could be mediated by the affinity of DVS to react with primary –OH and $–NH_2$ as well as their concentration within the $(PAH\text{-}HA)_{30}$ based hydrogels. The different partitions of both components clearly showed the different reaction mechanisms of both cross linkers, and can be used further to control the chemical features of the obtained hydrogel. However, the mechanical analyses performed on $(PAH\text{-}HA)_{30}$ cross-linked by DVS as reported in **Table 3** evidenced that the latter is significantly softer than the pure PAH-DVS hydrogel (*i.e.* almost 4 times softer) and appeared to be in the same stiffness range than HA-DVS hydrogel. The mechanical contribution of HA-DVS is dominating within the system $(PAH\text{-}HA)_{30}$ cross-linked by DVS. Such a result is not agreement with the mixing coefficient determined from chemometric analyses as reported in **Figure 7b**. Here, the mechanical feature of $(PAH\text{-}HA)_{30}$ cross-linked by DVS can be described as a linear mechanical combination of HA-DVS and PAH-DVS hydrogels with a partition of about 95% and 5% respectively. Such discrepancy between mechanical and chemical features could be explained by the occurrence of much more pending DVS on the PAH chains than on the HA chains as expected in the PEM as illustrated by **Figure S3**. Indeed, the very high reactivity of DVS probably allows the formation of a covalent bond at one of its ends with the HA and PAH chains, but does not leave enough time for the other end to react with another chain. On the other hand, DVS is a smaller molecule than BDDE and could possibly react with two neighboring amine functions on the same PAH chain.

This self-linking would then have a very small contribution to the mechanical properties within the polyelectrolyte network as well as the pending DVS.

Conclusion

In this work, we demonstrated by infrared measurements that the cross-linking of multilayered $(PAH\text{-}HA)_{30}$ based hydrogels with two different cross-linker agents (BDDE and DVS) led to significantly different chemical features. We also evidenced that the similar stiffnesses can be obtained for DVS concentrations up to 5 times lower than with BDDE concentrations (e.g. (PAH-HA)30 based hydrogel crosslinked with 1000 or 50 mM BDDE exhibit stiffness very close to the ones crosslinked with 250 or 10 mM DVS, respectively). Infrared analyses highlighted that BDDE reactivity toward primary alcohol and amine groups was significantly weaker and slower than the DVS ones. Furthermore, our results demonstrated that BDDE has much more affinity to react with primary alcohols than primary amino groups. Conversely, DVS tends to react preferentially to primary amino groups. We also evidenced by chemometric and statistical methods that the infrared fingerprint of $(PAH\text{-}HA)_{30}$ cross-linked with either BDDE or DVS can be described by a linear combination of pure spectral fingerprints of HA-BDDE, PAH-BDDE or HA-DVS, PAH-DVS based hydrogels. We calculated mixing coefficient ratios of 80% and 16% for $(PAH\text{-}HA)_{30}$ cross-linked with BDDE, and 55% and 45% for $(PAH\text{-}HA)_{30}$ cross-linked with DVS. Such different partitions could be explained by the peculiar layer-by-layer construction of $(PAH\text{-}HA)_{30}$ based hydrogels. Indeed, the cross-linking of this layered structure should lead to the presence of superimposition of layers enriched in only HA-BDDE or HA-DVS with layers enriched in only PAH-BDDE or PAH-DVS. It can be also hypothesized the occurrence of mixed layers containing HA and PAH chains linked together by BDDE or DVS at the interface between two successive layers. The mechanical analyses of $(PAH\text{-}HA)_{30}$ based hydrogels cross-linked at several concentrations evidenced that the mechanical contribution of HA was significantly lower than the mechanical contribution of PAH. Besides, these mechanical contributions were not totally in line with the mixing ratio calculated from infrared fingerprint of the cross-linked system. Indeed, $(PAH\text{-}HA)_{30}$ crosslinked with BDDE exhibited a high mechanical contribution of HA-BDDE in accordance with the chemometric unmixing method. However, this linear combination did not match with $(PAH\text{-}HA)_{30}$ crosslinked with DVS. The resulting crosslinked PEM was softer than expected, regarding the chemical contributions of HA-DVS and PAH-DVS. Our results show that it is possible to control the mechanical and chemical features by the choice of the crosslinkers alone or in the mixture.

Acknowledgements

The authors are indebted to the financial support of Région Grand Est for ERMES project under the reference FRCR2020. The authors thank the Spectroscopy and Microscopy Service Facility (SMI) of LCPME (Université de Lorraine-CNRS – http://www.lcpme.cnrs-nancy.fr) for physicochemical analyses including IR and AFM.

Supporting Information

Scheme 1.

Synopsis of $(PAH\text{-}HA)_{30}$ based hydrogel from build-up to cross-linking procedures.

Scheme 2.

Chemical reaction of 1,4-butanediol diglycidyl ether (BDDE) in panel a) and divinyl sulfone (DVS) in panel b) with respectively HA and PAH under alkaline conditions. Effective cross-linking corresponds to coupling/bridging between polymer chains (in red) whereas pending linking corresponds to side grafting to polymer (in blue).

Table S1.

Structures and specifications of the polyelectrolytes and cross-linking reagents (nd : not determined).

Table S2. Assignments of main infrared bands in the fingerprint region of hyaluronic acid (HA), polyallylamine (PAH), 1,4-Butanediol diglycidyl ether (BDDE), and divinyl sulfone (DVS) in aqueous solution. Key: δ, bending; υ, stretching; ρ, rocking, a, antisymmetric; s, symmetric, ip, in plane; oop, out of plane.

Table S3. Concentration parameters determined from calibration curves for BDDE according integration of 892-921 and 1236-1275 cm^{-1} regions corresponding to νs and νa epoxy ring respiration, respectively. Concentration parameters determined from calibration curves for DVS according integration of 975-1000 and 1095-1147 cm^{-1} regions corresponding to δipCH and νs SO_2, respectively. Concentration parameters determined from calibration curves for HA according integration of 912-1190 and 1410-1431 cm^{-1} regions corresponding to νC-O-C, νC-OH, νC-C, νC-O-C and νsCOO^-, respectively. Concentration parameter determined from calibration curves for PAH according integration of 1483-1573 cm^{-1} region corresponding to δsNH_3^+.

Figure S1. (a) comparison of the experimental spectra of HA (100 g/L in water) and PAH (50 g/L in water) with the two estimated sources obtained by BPSS unmixing algorithm. (b) Evolution of the mixing coefficients (triangles) and the ratio of both series (squares) during the hydrogel build-up as a function of the number of deposited bilayers of (PAH-HA) and determined by BPSS method.

Figure S2. Chemical reaction of 1,4-Butanediol diglycidyl ether (BDDE) with respectively HA and PAH under alkaline conditions. Effective crosslinking corresponds to coupling/bridging between polymer chains (in red) whereas pending linking corresponds to side grafting to polymer (in blue).

Figure S3. Chemical reaction of divinyl sulfone (DVS) with HA and PAH, respectively, under alkaline conditions. Effective crosslinking corresponds to coupling/bridging between polymer chains (in red) whereas pending linking corresponds to side grafting to polymer (in blue).

Figure S4. Height images of $(PAH\text{-}HA)_{30}$ in air before (a, g) and after crosslinking with BDDE at 50, 250, 500, 1000 or 1500 mM (b-f). AFM images of $(PAH\text{-}HA)_{30}$ in NaCl, TRIS buffer after crosslinking with DVS at 50, 100, 250, 500 and 1000 mM. AFM images were recorded using peakforce tapping mode in air.

Figure S5. Evolution of the thickness of $(PAH\text{-}HA)_{30}$ based hydrogel as function of cross-linker concentration in under aqueous (a) and dried conditions (b). Data were collected from the analyses of AFM images of hydrogel scratches (about 20 µm alongside).

Figure S6. Evolution of the mechanical properties of HA-BDDE, PAH-BDDE and $(PAH\text{-}HA)_{30}$ crosslinked with BDDE as a function of the BDDE concentration (a). Evolution of the mechanical properties of HA-DVS, PAH-DVS and $(PAH\text{-}HA)_{30}$ crosslinked with DVS (b) as a function of DVS concentration. Blue bars correspond to HA-BDDE and HA-DVS, green bars correspond to PAH-BDDE and PAH-DVS, and violet bars correspond to (PAH-HA)30 crosslinked with BDDE and DVS respectively.

References

1. *Antimicrobial Coatings Market Size And Forecast*; Report ID: 32266; Verified Market Research: 2022.

2. Mitra, D.; Kang, E.-T.; Neoh, K. G., Chapter 20 - Applications and challenges of smart antibacterial coatings. In *Advances in Smart Coatings and Thin Films for Future Industrial and Biomedical Engineering Applications*, Makhlouf, A. S. H.; Abu-Thabit, N. Y., Eds. Elsevier: 2020; pp 537-556.

3. Salwiczek, M.; Qu, Y.; Gardiner, J.; Strugnell, R. A.; Lithgow, T.; McLean, K. M.; Thissen, H., Emerging rules for effective antimicrobial coatings. *Trends Biotechnol.* **2014,** *32*, 82-90.

4. Tallet, L.; Gribova, V.; Ploux, L.; Vrana, N. E.; Lavalle, P., New Smart Antimicrobial Hydrogels, Nanomaterials, and Coatings: Earlier Action, More Specific, Better Dosing? *Adv. Healthc. Mater.* **2021,** *10*, 2001199.

5. Cloutier, M.; Mantovani, D.; Rosei, F., Antibacterial Coatings: Challenges, Perspectives, and Opportunities. *Trends Biotechnol.* **2015,** *33*, 637-652.

6. Hartmann, H.; Krastev, R., Biofunctionalization of surfaces using polyelectrolyte multilayers. *BioNanoMaterials* **2017,** *18*, 20160015.

7. Petrila, L.-M.; Bucatariu, F.; Mihai, M.; Teodosiu, C., Polyelectrolyte Multilayers: An Overview on Fabrication, Properties, and Biomedical and Environmental Applications. *Materials* **2021,** *14*, 4152.

8. Liu, X.; Li, Y.; Li, S.; Lin, Y.-C.; Li, V. L.; Chen, Y.-H.; Lin, C.; Keerthi, M.; Shih, S.-J.; Chung, R.-J., Polyelectrolyte multilayer coatings for short/long-term release of antibacterial agents. *Surf. Coat. Technol.* **2020,** *393*, 125696.

9. Seon, L.; Lavalle, P.; Schaaf, P.; Boulmedais, F., Polyelectrolyte Multilayers: A Versatile Tool for Preparing Antimicrobial Coatings. *Langmuir* **2015,** *31*, 12856-72.

10. Pahal, S.; Gakhar, R.; Raichur, A.; Varma, M., Polyelectrolyte Multilayers for Bio-applications: Recent Advancements. *IET Nanobiotechnology* **2017,** *11*, 903–908.

11. Ghiorghita, C.-A.; Bucatariu, F.; Dragan, E. S., Influence of cross-linking in loading/release applications of polyelectrolyte multilayer assemblies. A review. *Mater. Sci. Eng. C* **2019,** *105*, 110050.

12. Alves, N. M.; Picart, C.; Mano, J. F., Self Assembling and Crosslinking of Polyelectrolyte Multilayer Films of Chitosan and Alginate Studied by QCM and IR Spectroscopy. *Macromol. Biosci.* **2009,** *9*, 776-785.

13. Imbir, G.; Trembecka-Wójciga, K.; Ozga, P.; Schirhagl, R.; Mzyk, A., Elastic moduli of polyelectrolyte multilayer films regulate endothelium-blood interaction under dynamic conditions. *Colloids Surf., B* **2023,** *225*, 113269.

14. Wang, L.-M.; Chang, H.; Zhang, H.; Ren, K.; Li, H.; Hu, M.; Li, B.-C.; Martins, M. C.; Barbosa, M.; Ji, J., Dynamic stiffness of polyelectrolyte multilayer films based on disulfide bonds for in situ control of cell adhesion. *Journal of Materials Chemistry B* **2015,** *3*, 7546-7553.

15. Fumasi, F. M.; Stephanopoulos, N.; Holloway, J. L., Reversible control of biomaterial properties for dynamically tuning cell behavior. *J. Appl. Polym. Sci.* **2020,** *137*, 1-16.

16. Pozos Vázquez, C.; Boudou, T.; Dulong, V.; Nicolas, C.; Picart, C.; Glinel, K., Variation of Polyelectrolyte Film Stiffness by Photo-Cross-Linking: A New Way To Control Cell Adhesion. *Langmuir* **2009,** *25*, 3556-3563.

17. Kamoun, E. A.; Kenawy, E. S.; Chen, X., A review on polymeric hydrogel membranes for wound dressing applications: PVA-based hydrogel dressings. *J Adv Res* **2017,** *8*, 217-233.

18. Liang, Y.; He, J.; Guo, B., Functional Hydrogels as Wound Dressing to Enhance Wound Healing. *ACS Nano* **2021,** *15*, 12687-12722.

19. Tavakoli, S.; Klar, A. S., Advanced Hydrogels as Wound Dressings. *Biomolecules* **2020,** *10*, 1169.

20. Liu, J.; Qu, S.; Suo, Z.; Yang, W., Functional hydrogel coatings. *National Science Review* **2020,** *8*, nwaa254.

21. Pérez-Köhler, B.; Pascual, G.; Benito-Martínez, S.; Bellón, J. M.; Eglin, D.; Guillaume, O., Thermo-Responsive Antimicrobial Hydrogel for the In-Situ Coating of Mesh Materials for Hernia Repair. *Polymers* **2020,** *12*, 1245.

22. Mihajlovic, M.; Fermin, L.; Ito, K.; van Nostrum, C. F.; Vermonden, T., Hyaluronic acid-based supramolecular hydrogels for biomedical applications. *Multifunctional Materials* **2021,** *4*, 032001.

23. Dovedytis, M.; Liu, Z. J.; Bartlett, S., Hyaluronic acid and its biomedical applications: A review. *Engineered Regeneration* **2020,** *1*, 102-113.

24. Khunmanee, S.; Jeong, Y.; Park, H., Crosslinking method of hyaluronic-based hydrogel for biomedical applications. *Journal of tissue engineering* **2017,** *8*, 2041731417726464.

25. Pérez, L. A.; Hernández, R.; Alonso, J. M.; Pérez-González, R.; Sáez-Martínez, V., Hyaluronic Acid Hydrogels Crosslinked in Physiological Conditions: Synthesis and Biomedical Applications. *Biomedicines* **2021,** *9*, 1113.

26. Lee, J. N.; Lee, S. Y.; Park, W. H., Bioinspired Self-Healable Polyallylamine-Based Hydrogels for Wet Adhesion: Synergistic Contributions of Catechol-Amino Functionalities and Nanosilicate. *ACS Appl. Mater. Interfaces* **2021,** *13*, 18324-18337.

27. Elsiddig, R.; O'Reilly, N. J.; Hudson, S. P.; Owens, E.; Hughes, H.; O'Grady, D.; McLoughlin, P., The influence of poly(allylamine hydrochloride) hydrogel crosslinking density on its thermal and phosphate binding properties. *Int. J. Pharm.* **2022,** *621*, 121806.

28. O'Connor, N. A.; Abugharbieh, A.; Yasmeen, F.; Buabeng, E.; Mathew, S.; Samaroo, D.; Cheng, H.-P., The crosslinking of polysaccharides with polyamines and dextran–polyallylamine antibacterial hydrogels. *Int. J. Biol. Macromol.* **2015,** *72*, 88-93.

29. Bui, T. Q.; Cao, V. D.; Do, N. B. D.; Christoffersen, T. E.; Wang, W.; Kjøniksen, A.-L., Salinity Gradient Energy from Expansion and Contraction of Poly(allylamine hydrochloride) Hydrogels. *ACS Appl. Mater. Interfaces* **2018,** *10*, 22218-22225.

30. Szarpak, A.; Pignot-Paintrand, I.; Nicolas, C.; Picart, C.; Auzély-Velty, R., Multilayer Assembly of Hyaluronic Acid/Poly(allylamine): Control of the Buildup for the Production of Hollow Capsules. *Langmuir* **2008,** *24*, 9767-9774.

31. Burke, S.; Barrett, C., Swelling Behavior of Hyaluronic Acid/Polyallylamine Hydrochloride Multilayer Films. *Biomacromolecules* **2005,** *6*, 1419-28.

32. Marais, A.; Utsel, S.; Gustafsson, E.; Wågberg, L., Towards a super-strainable paper using the Layer-by-Layer technique. *Carbohydr. Polym.* **2014,** *100*, 218-224.

33. Ciejka, J.; Grzybala, M.; Gut, A.; Szuwarzynski, M.; Pyrc, K.; Nowakowska, M.; Szczubiałka, K., Tuning the Surface Properties of Poly(Allylamine Hydrochloride)-Based Multilayer Films. *Materials* **2021,** *14*, 2361.

34. Li, X.; Sun, Q.; Li, Q.; Kawazoe, N.; Chen, G., Functional Hydrogels With Tunable Structures and Properties for Tissue Engineering Applications. *Frontiers in Chemistry* **2018,** *6*, 499.

35. Xue, B.; Tang, D.; Wu, X.; Xu, Z.; Gu, J.; Han, Y.; Zhu, Z.; Qin, M.; Zou, X.; Wang, W.; Cao, Y., Engineering hydrogels with homogeneous mechanical properties for controlling stem cell lineage specification. *Proc Natl Acad Sci. USA* **2021,** *118*, e2110961118.

36. Yang, B.; Wei, Z.; Chen, X.; Wei, K.; Bian, L., Manipulating the mechanical properties of biomimetic hydrogels with multivalent host–guest interactions. *Journal of Materials Chemistry B* **2019,** *7*, 1726-1733.

37. Oyen, M. L., Mechanical characterisation of hydrogel materials. *Int. Mater. Rev.* **2014,** *59*, 44-59.

38. Francius, G.; Hemmerle, J.; Voegel, J. C.; Schaaf, P.; Senger, B.; Ball, V., Anomalous thickness evolution of multilayer films made from poly-L-lysine and mixtures of hyaluronic acid and polystyrene sulfonate. *Langmuir* **2007,** *23*, 2602-7.

39. Schneider, A.; Francius, G.; Obeid, R.; Schwinte, P.; Hemmerle, J.; Frisch, B.; Schaaf, P.; Voegel, J. C.; Senger, B.; Picart, C., Polyelectrolyte multilayers with a tunable Young's modulus: influence of film stiffness on cell adhesion. *Langmuir* **2006,** *22*, 1193-200.

40. Benbow, N. L.; Webber, J. L.; Pawliszak, P.; Sebben, D. A.; Ho, T. T. M.; Vongsvivut, J.; Tobin, M. J.; Krasowska, M.; Beattie, D. A., A Novel Soft Contact Piezo-Controlled Liquid Cell for Probing Polymer Films under Confinement using Synchrotron FTIR Microspectroscopy. *Sci Rep* **2018,** *8*, 17804.

41. Dobigeon, N.; Moussaoui, S.; Tourneret, J.-Y.; Carteret, C., Bayesian separation of spectral sources under non-negativity and full additivity constraints. *Signal Process.* **2009,** *89*, 2657-2669.

42. Moussaoui, S.; Carteret, C.; Brie, D.; Mohammad-Djafari, A., Bayesian analysis of spectral mixture data using Markov Chain Monte Carlo Methods. *Chemom. Intell. Lab. Syst.* **2006,** *81*, 137-148.

43. Moussaoui, S.; Brie, D.; Mohammad-Djafari, A.; Carteret, C., Separation of Non-Negative Mixture of Non-Negative Sources Using a Bayesian Approach and MCMC Sampling. *IEEE Transactions on Signal Processing* **2006,** *54*, 4133-4145.

44. Yunda, E.; Quilès, F., In situ spectroscopic analysis of Lactobacillus rhamnosus GG flow on an abiotic surface reveals a role for nutrients in biofilm development. *Biofouling* **2019,** *35*, 494-507.

45. Quilès, F.; Nguyen-Trung, C.; Carteret, C.; Humbert, B., Hydrolysis of Uranyl(VI) in Acidic and Basic Aqueous Solutions Using a Noncomplexing Organic Base: A Multivariate Spectroscopic and Statistical Study. *Inorg. Chem.* **2011,** *50*, 2811-2823.

46. Carteret, C.; Dandeu, A.; Moussaoui, S.; Muhr, H.; Humbert, B.; Plasari, E., Polymorphism Studied by Lattice Phonon Raman Spectroscopy and Statistical Mixture Analysis Method. Application to Calcium Carbonate Polymorphs during Batch Crystallization. *Cryst. Growth Des.* **2009,** *9*, 807-812.

47. Sneddon, I. N., The relation between load and penetration in the axisymmetric Boussinesq problem for a punch of arbitrary profile. *Int. J. Eng. Sci.* **1965,** *3*, 47-57.

48. Gavara, N.; Chadwick, R. S., Determination of the elastic moduli of thin samples and adherent cells using conical atomic force microscope tips. *Nat. Nanotechnol.* **2012,** *7*, 733-6.

49. Polyakov, P.; Soussen, C.; Duan, J. B.; Duval, J. F. L.; Brie, D.; Francius, G., Automated Force Volume Image Processing for Biological Samples. *PLoS One* **2011,** *6*, e18887.

50. Haxaire, K.; Marechal, Y.; Milas, M.; Rinaudo, M., Hydration of polysaccharide hyaluronan observed by IR spectrometry. I. Preliminary experiments and band assignments. *Biopolymers* **2003,** *72*, 10-20.

51. Ouasri, A.; Rhandour, A.; Dhamelincourt, M.-C.; Dhamelincourt, P.; Mazzah, A., The infrared and Raman spectra of ethylammonium hexafluorosilicate [C2H5NH3]2SiF6. *Spectrochimica Acta Part A: Molecular and Biomolecular Spectroscopy* **2003,** *59*, 357-362.

52. Zeroka, D.; Jensen, J. O.; Samuels, A. C., Infrared spectra of some isotopomers of ethylamine and the ethylammonium ion: a theoretical study. *Journal of Molecular Structure: THEOCHEM* **1999,** *465*, 119-139.

53. Diziain, S.; Dejeu, J.; Buisson, L.; Charraut, D.; Membrey, F.; Foissy, A., Investigations in the initial build-up stages of polyelectrolyte multilayers by laser reflectometry and atomic force microscopy. *Thin Solid Films* **2007,** *516*, 1-7.

54. Zhang, J.; Senger, B.; Vautier, D.; Picart, C.; Schaaf, P.; Voegel, J. C.; Lavalle, P., Natural polyelectrolyte films based on layer-by layer deposition of collagen and hyaluronic acid. *Biomaterials* **2005,** *26*, 3353-61.

55. Lai, J. Y., Relationship between structure and cytocompatibility of divinyl sulfone cross-linked hyaluronic acid. *Carbohydr. Polym.* **2014,** *101*, 203-12.

56. Zeeman, R.; Dijkstra, P. J.; van Wachem, P. B.; van Luyn, M. J.; Hendriks, M.; Cahalan, P. T.; Feijen, J., Crosslinking and modification of dermal sheep collagen using 1, 4-butanediol diglycidyl ether. *J Biomed Mater Res* **1999,** *46*, 424-33.

57. Colthup, N.; Daly, L.; Wiberley, S., *Introduction to Infrared and Raman Spectroscopy*. 3rd Edition ed.; 1990; p 547.

58. Kenne, L.; Gohil, S.; Nilsson, E. M.; Karlsson, A.; Ericsson, D.; Helander Kenne, A.; Nord, L. I., Modification and cross-linking parameters in hyaluronic acid hydrogels—Definitions and analytical methods. *Carbohydr. Polym.* **2013,** *91*, 410-418.

59. Hua, J.; Li, Z.; Xia, W.; Yang, N.; Gong, J.; Zhang, J.; Qiao, C., Preparation and properties of EDC/NHS mediated crosslinking poly (gamma-glutamic acid)/epsilon-polylysine hydrogels. *Materials science & engineering. C, Materials for biological applications* **2016,** *61*, 879-92.

60. Lu, P. L.; Lai, J. Y.; Ma, D. H.; Hsiue, G. H., Carbodiimide cross-linked hyaluronic acid hydrogels as cell sheet delivery vehicles: characterization and interaction with corneal endothelial cells. *J Biomater Sci Polym Ed* **2008,** *19*, 1-18.

61. Panja, S.; Adams, D. J., Chemical crosslinking in 'reactive' multicomponent gels. *Chem Commun (Camb)* **2022,** *58*, 5622-5625.

62. Zeeman, R.; Dijkstra, P. J.; van Wachem, P. B.; van Luyn, M. J.; Hendriks, M.; Cahalan, P. T.; Feijen, J., The kinetics of 1,4-butanediol diglycidyl ether crosslinking of dermal sheep collagen. *J Biomed Mater Res* **2000,** *51*, 541-8.

63. Mezzenga, R.; Boogh, L.; Månson, J.-A. E.; Pettersson, B., Effects of the Branching Architecture on the Reactivity of Epoxy−Amine Groups. *Macromolecules* **2000,** *33*, 4373-4379.

Graphical abstract

$(PAH/HA)_{30}$ cross-linked by BDDE

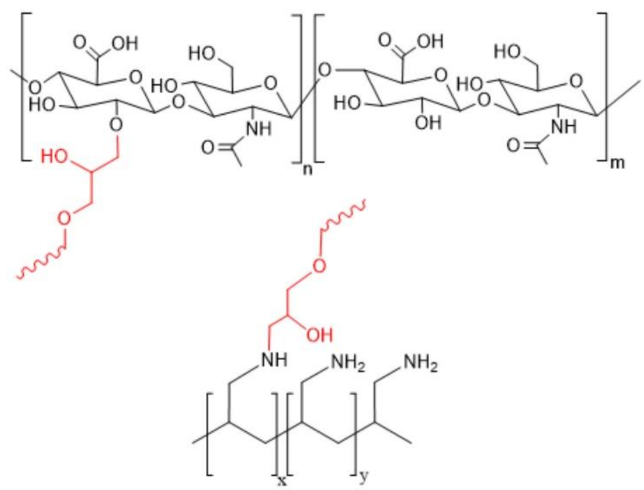

$(PAH/HA)_{30}$ cross-linked by DVS

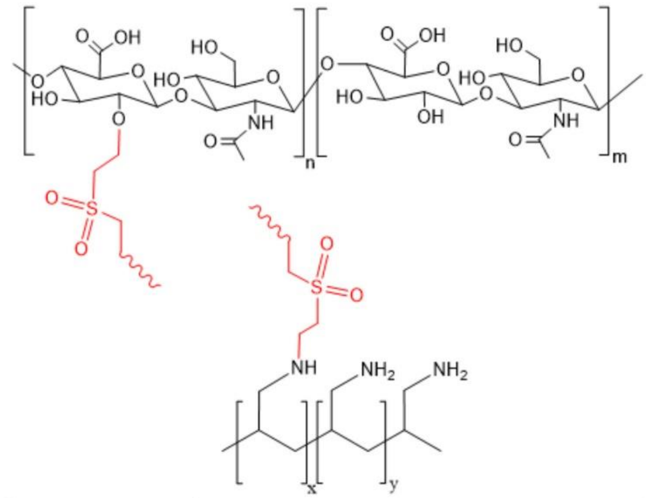

Features	Mixing coefficients	
	HA-BDDE	PAH-BDDE
Chemical	~80%	~16%
Mechanical	~ 66%	~33%

Features	Mixing coefficients	
	HA-DVS	PAH-DVS
Chemical	~55%	~45%
Mechanical	~95%	~5%

List of tables

Table 1.

Kinetic parameters for the crosslinking reaction of $(PAH\text{-}HA)_{30}$ film with BDDE and DVS (upper panel), and for HA and PAH hydrogels formations using BDDE and DVS (lower panel). These parameters were calculated from infrared data reported in **Figures 2 and 6**.

$(PAH\text{-}HA)_{30}$ crosslinked with BDDE			
Parameters	**HA**	**PAH**	**BDDE**
C_0 **(Mixing coef. %)**	23.82±0.21	0.00	77.32±0.50
C_1 **(Mixing coef. %)**	36.60±0.32	22.065±0.51	-59.07±0.64
k **(h^{-1})**	0.32±0.01	0.24±0.01	0.27±0.01
t^* **(h)**	3.14±0.09	4.11±0.22	3.75±0.13

Hydrogels obtained with BDDE		
Parameters	**HA**	**PAH**
C_0 **(mM)**	653.43±21.65	0.00
C_1 **(mM)**	447.71±18.19	1135.69±73.96
k **(h^{-1})**	0.08±0.01	0.04±0.01
t^* **(h)**	13.20±1.41	26.66±4.43

$(PAH\text{-}HA)_{30}$ crosslinked with DVS			
Parameters	**HA**	**PAH**	**DVS**
C_0 **(Mixing coef. %)**	18.32±0.40	0.16±0.05	80.93±0.42
C_1 **(Mixing coef. %)**	19.06±0.81	4.23±0.65	-21.45±1.19
k **(h^{-1})**	0.44±0.05	5.21±1.09	0.65±0.01
t^* **(h)**	2.29±0.28	0.19±0.04	1.54±0.21

Hydrogels obtained with DVS		
Parameters	**HA**	**PAH**
C_0 **(mM)**	50.81±3.17	72.05±0.78
C_1 **(mM)**	203.39±11.29	187.11±4.57
k **(h^{-1})**	4.70±0.51	41.67±3.47
t^* **(h)**	0.21±0.02	0.02±0.00

Table 2.

Mechanical and morphological properties of $(PAH\text{-}HA)_{30}$ based hydrogel before and after its crosslinking with BDDE, DVS or EDC at several concentrations. Data were obtained from nanoindentation measurements and AFM images reported in supporting information (**Figure S4**).

BDDE concentration	**0 mM**	**5 mM**	**50 mM**	**250 mM**	**500 mM**	**1 M**	**1.5 M**
Stiffness (kPa)	7.7±2.0	8.8±3.4	13.2±1.9	35.5±9.8	51.2±19.8	79.4±31.5	137.8±36.1
Stiffening ratio	--	1.14	1.72	4.60	6.65	10.31	17.89
Thickness (µm)	4.17±0.08	3.34±0.25	3.21±0.27	3.11±0.15	2.95 ±0.11	2.91±0.16	2.78±0.09
Roughness (nm)	7.2±3.3	9.7±3.1	6.6±2.0	10.7±2.5	16.5±4.7	21.4±5.6	23.5±6.1
Swelling ratio	9.10	8.27	5.06	4.58	4.45	3.50	2.97
DVS concentration	**0 mM**	**10 mM**	**50 mM**	**100 mM**	**250 mM**	**500 mM**	**1 M**
Stiffness (kPa)	8.1±0.3	17.2±2.4	41.1±6.1	67.6±10.1	102.5±9.1	174.1±31.3	250.6±39.7
Stiffening ratio	--	2.12	5.07	8.33	12.63	21.46	30.89
Thickness (µm)	4.62±0.11	4.49±0.33	4.57±0.29	4.75±0.24	4.59±0.18	4.68±0.15	4.67±0.20
Roughness (nm)	7.6±1.8	10.5±2.5	8.3±1.7	8.0±2.1	6.0 ±2.1	8.5±2.6	7.9±1.9
Swelling ratio	8.73	3.98	3.85	3.03	3.14	2.89	2.18
EDC concentration	**3.2 mM**	**16 mM**	**50 mM**	**100 mM**	**250 mM**	**500 mM**	**1 M**
Stiffness (kPa)	37.3±14.7	172.4±51.6	363±44.8	395±43	685±57	786±90	817±72
Stiffening ratio	4.6	19.8	44.7	46.3	84.53	96.9	100.8
Thickness (µm)	4.29±0.13	4.15±0.10	4.02±0.18	4.20 ±0.22	3.98±0.27	4.18±0.13	3.39±0.09
Roughness (nm)	4.94	3.78	3.15	2.94	2.77	2.24	1.98

Table 3.

Mechanical properties of HA, PAH and (PAH-HA)$_{30}$ based hydrogels obtained by crosslinking with BDDE or DVS at 500 and 1000 mM concentrations. Data were obtained from AFM measurements according to the nanoindentation technique.

Cross-linking agents	**Mechanical properties after 24 h cross-linking reaction (kPa)**		
BDDE	**HA**	**PAH**	**(PAH-HA)$_{30}$**
500 mM	0.6±0.1	179.8±28.9	51.2±19.8
1000 mM	3.4±0.8	238.4±74.7	79.4±31.5
DVS	**HA**	**PAH**	**(PAH-HA)$_{30}$**
500 mM	106.5±33.2	284.4±121.6	102.5±9.1
1000 mM	151.0±47.5	629.7±173.5	174.1±31.3

List of Figures

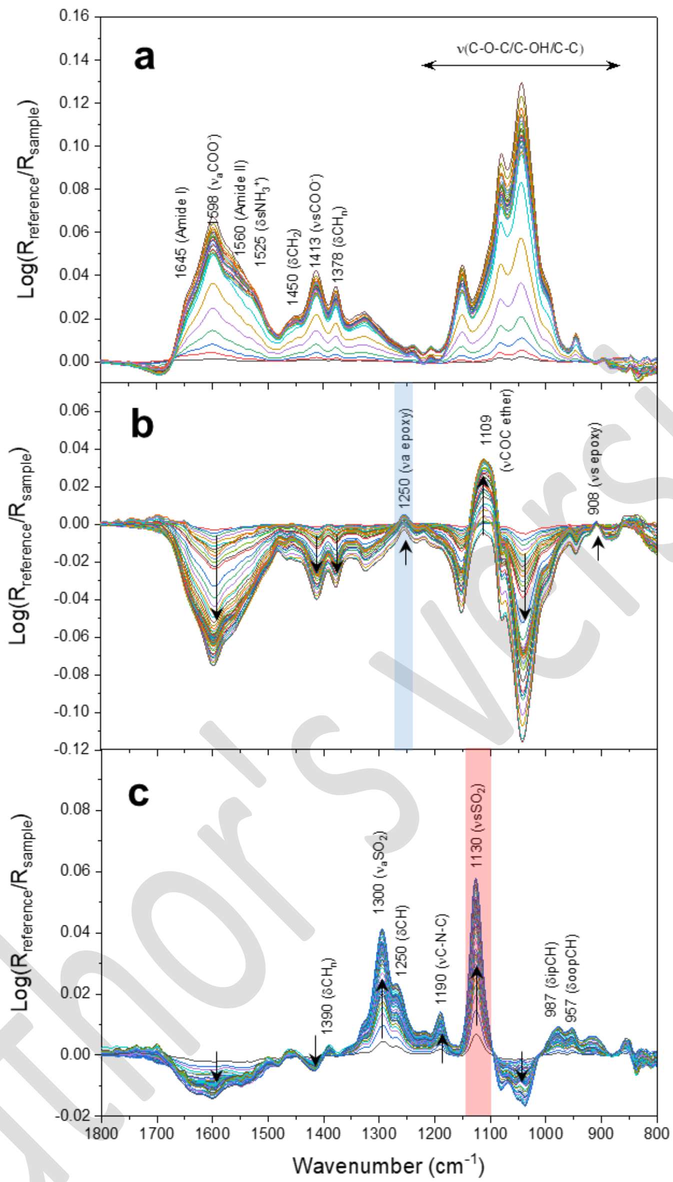

Figure 1. ATR-FTIR spectra of (a) (PAH-HA)$_{30}$ based hydrogel during the LbL build-up, reference spectrum is NaCl, TRIS buffer. (b) and (c) panels correspond to the time evolutions of differential spectra of (PAH-HA)$_{30}$ based hydrogel during its crosslinking with BDDE (1000 mM) or DVS (250 mM), reference spectrum is (PAH-HA)$_{30}$ based hydrogel just before exposure to BDDE or DVS, respectively. Vertical arrows show the evolution of the intensity of the considered bands as a function of time.

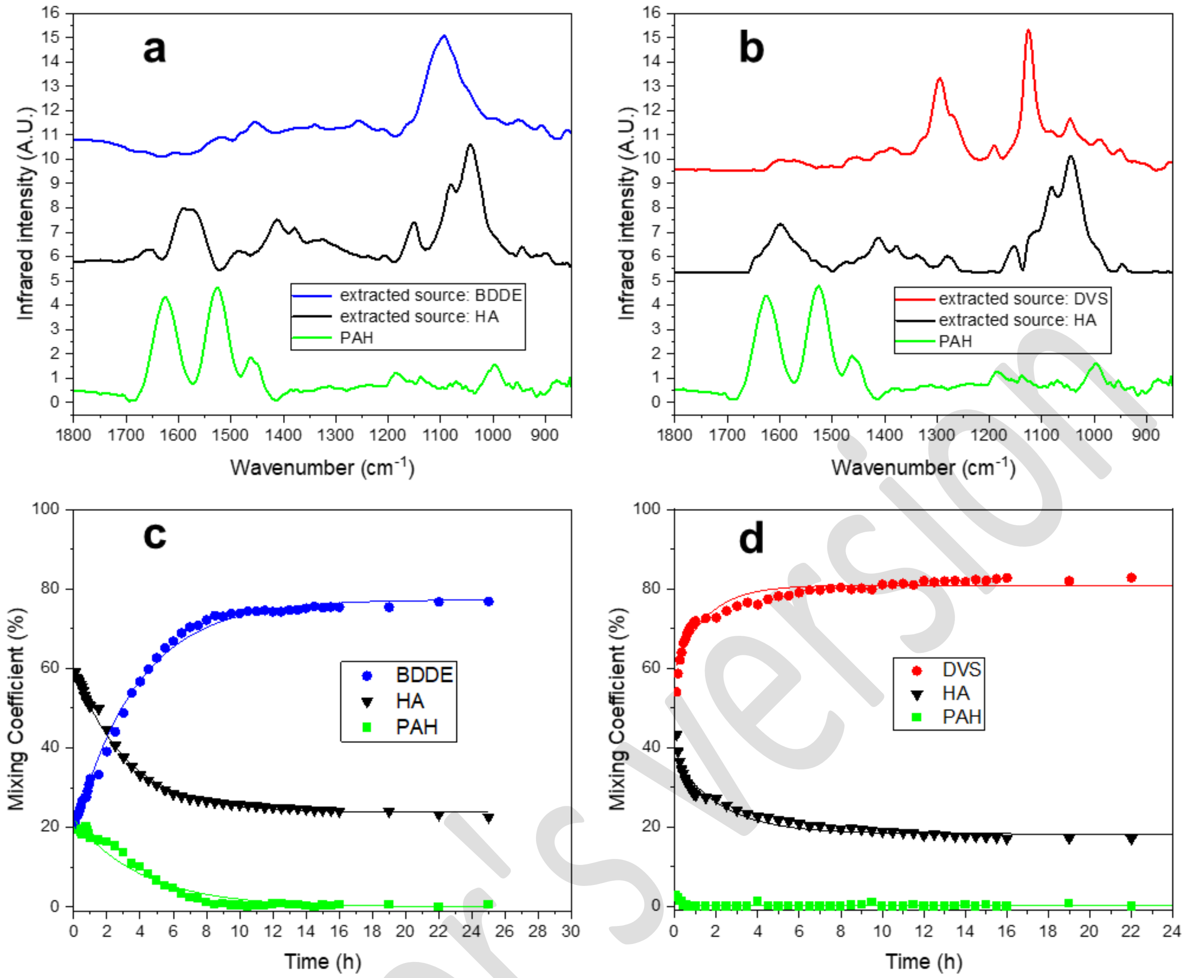

Figure 2. Estimated BPSS ATR-FTIR pure component spectra from the spectra recorded during the crosslinking of $(PAH\text{-}HA)_{30}$ based hydrogel with BDDE (a) or DVS (b). The reference spectrum is NaCl, TRIS buffer. The spectrum of pure PAH in solution was imposed as a source, and they were additional two free sources in the calculations. Vertical shift of spectra is used for clarity. Corresponding relative mixing coefficients profiles (c, d). Evolution of unreacted PAH (green squares), unreacted HA (black down triangles), consumed BDDE (blue circles) and consumed DVS (red circles).

.

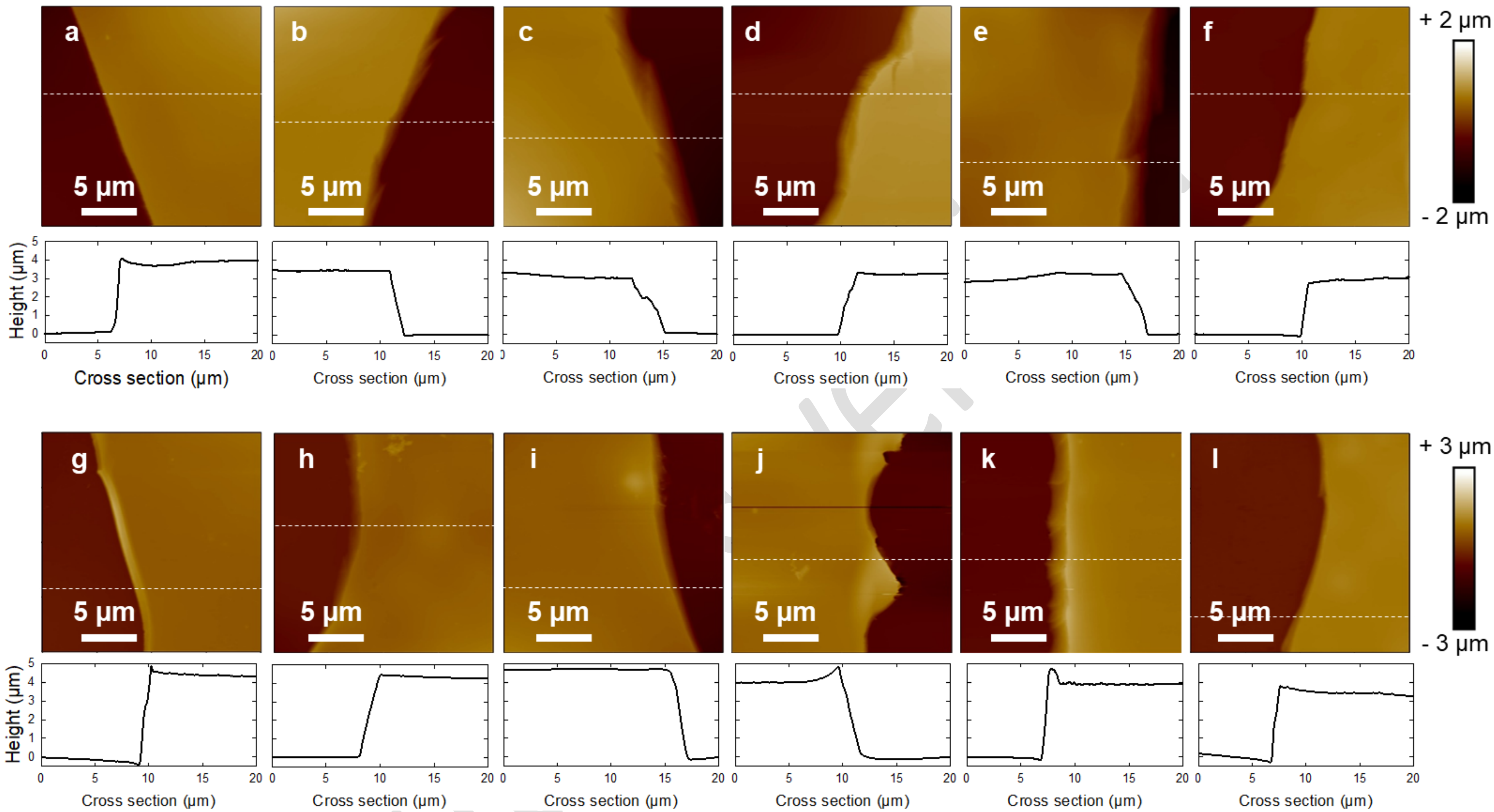

Figure 3. AFM height images of (PAH-HA)$_{30}$ in NaCl, TRIS buffer before (a, g) and after crosslinking with BDDE at 50, 250, 500, 1000 or 1500 mM (b-f). AFM images of (PAH-HA)$_{30}$ in NaCl, TRIS buffer after crosslinking with DVS at 50, 100, 250, 500 or 1000 mM (h-l). AFM images were recorded using peakforce tapping mode in aqueous medium. Lower panels under AFM images correspond to the cross-section taken from the white dashed line.

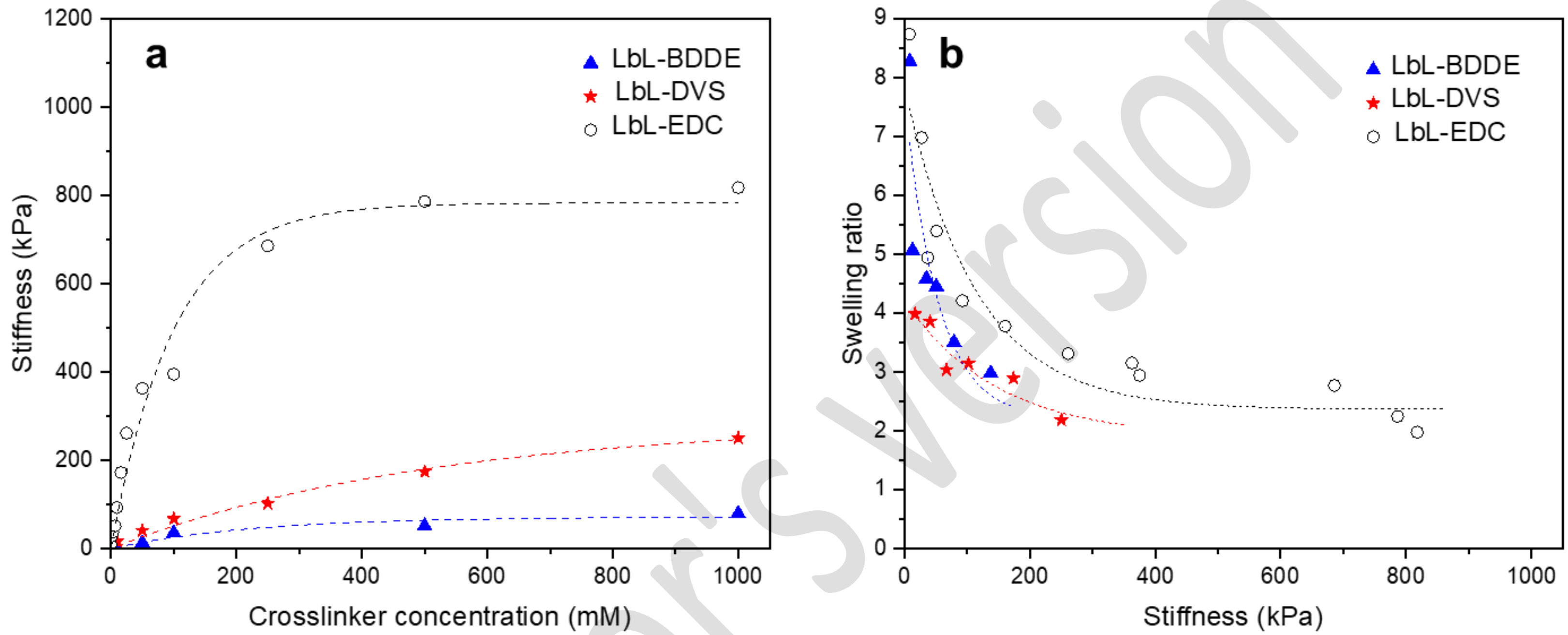

Figure 4. Evolution of (a) mechanical stiffness and (b) swelling ratio of $(PAH\text{-}HA)_{30}$ based hydrogel according to the crosslinking procedure at several concentrations of BDDE (blue triangle), DVS (red stars) or EDC (white circles). Trend curves are shown for the eye only.EDC crosslinking of $(PAH\text{-}HA)_{30}$ based hydrogels was done using various EDC concentration mixed with NHS at 10 mM.

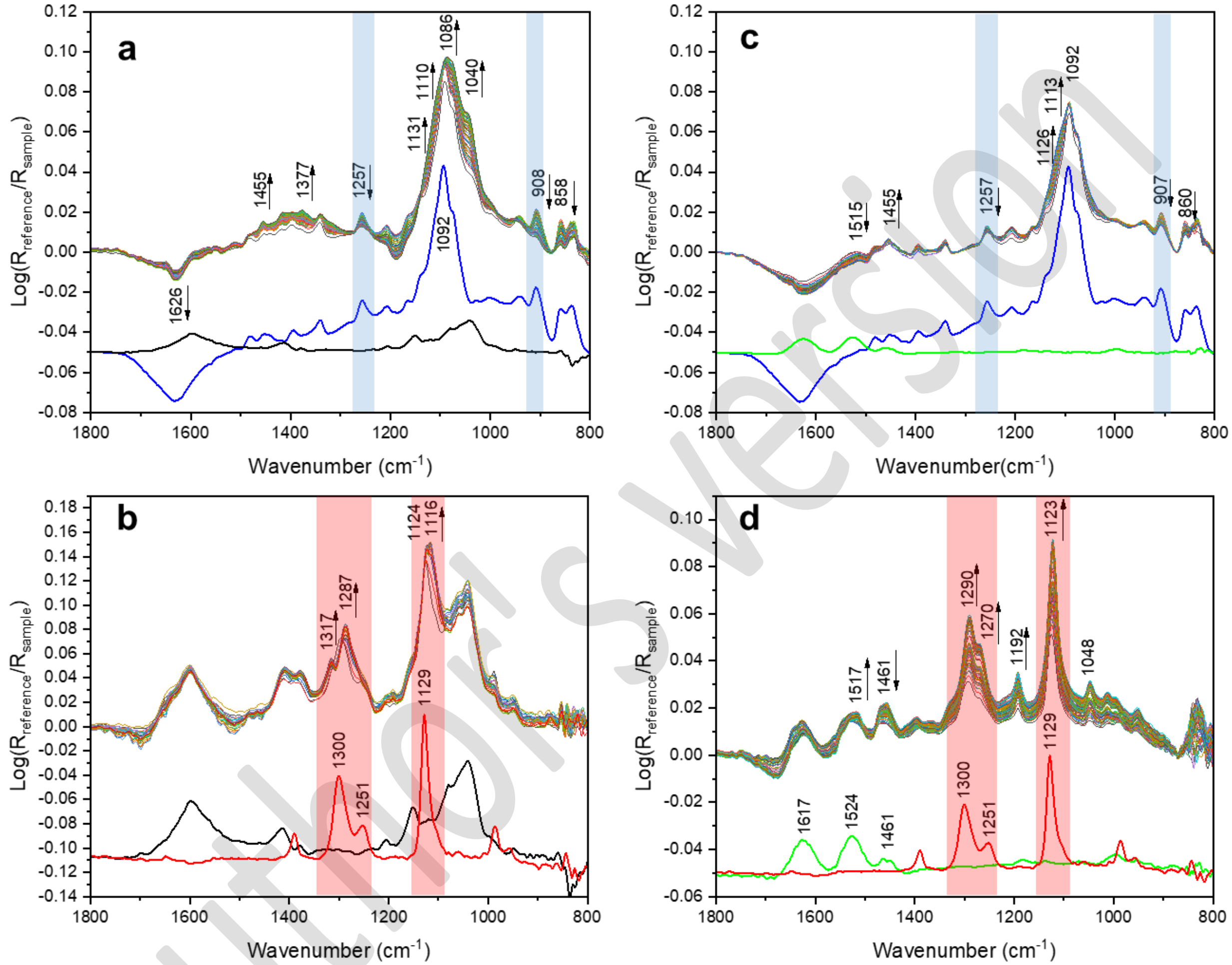

Figure 5. ATR-FTIR spectra of HA (a, b) and PAH (c, d) hydrogels during their formation by crosslinking with BDDE (a, c) or DVS (b, d). Reference spectrum is NaCl, TRIS buffer (150 mM, 10 mM at pH 10). Initial concentrations are 50 g/L for HA and PAH, 1000 mM for BDDE, and 250 mM for DVS.

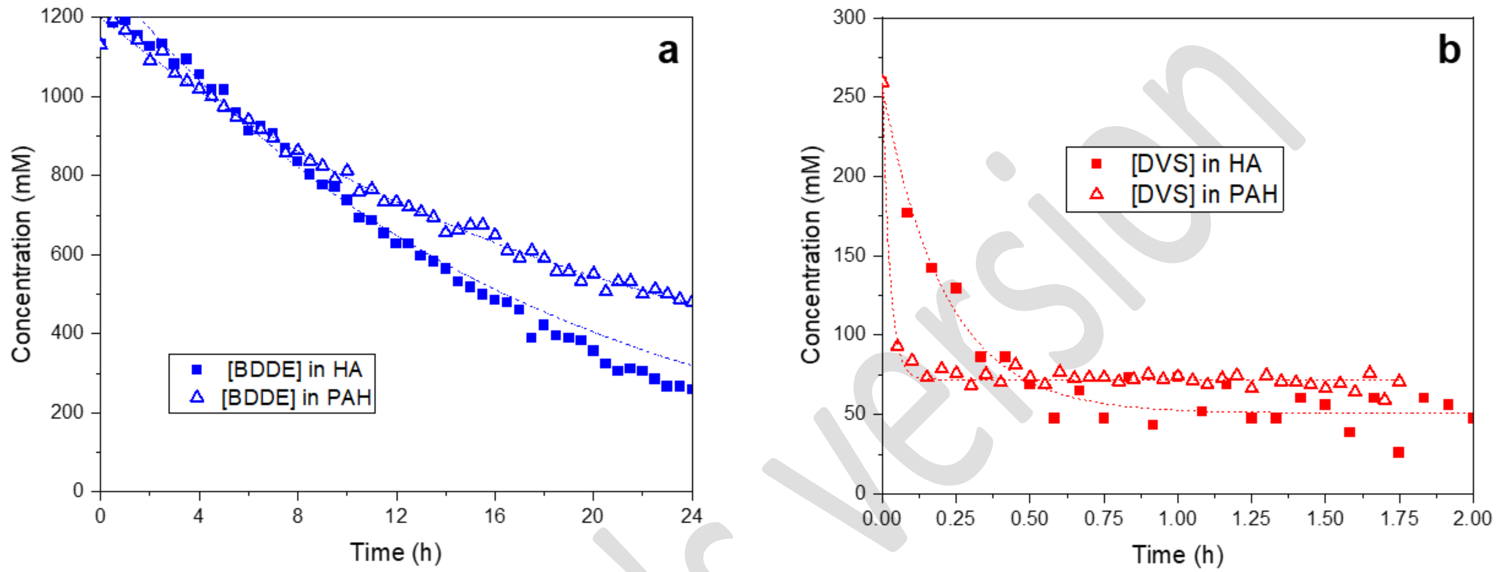

Figure 6. Time-evolution of BDDE (a) and DVS (b) for HA (squares) and PAH (open triangles) during hydrogels formation. Hydrogels were obtained by crosslinking with either BDDE or DVS, respectively. Concentrations of consumed BDDE were determined from integrated intensities between 892-921 cm^{-1}. Concentrations of consumed DVS were determined from integrated intensities between 972-1000 and 1354-1428 cm^{-1} for HA-DVS and PAH-DVS hydrogels, respectively.

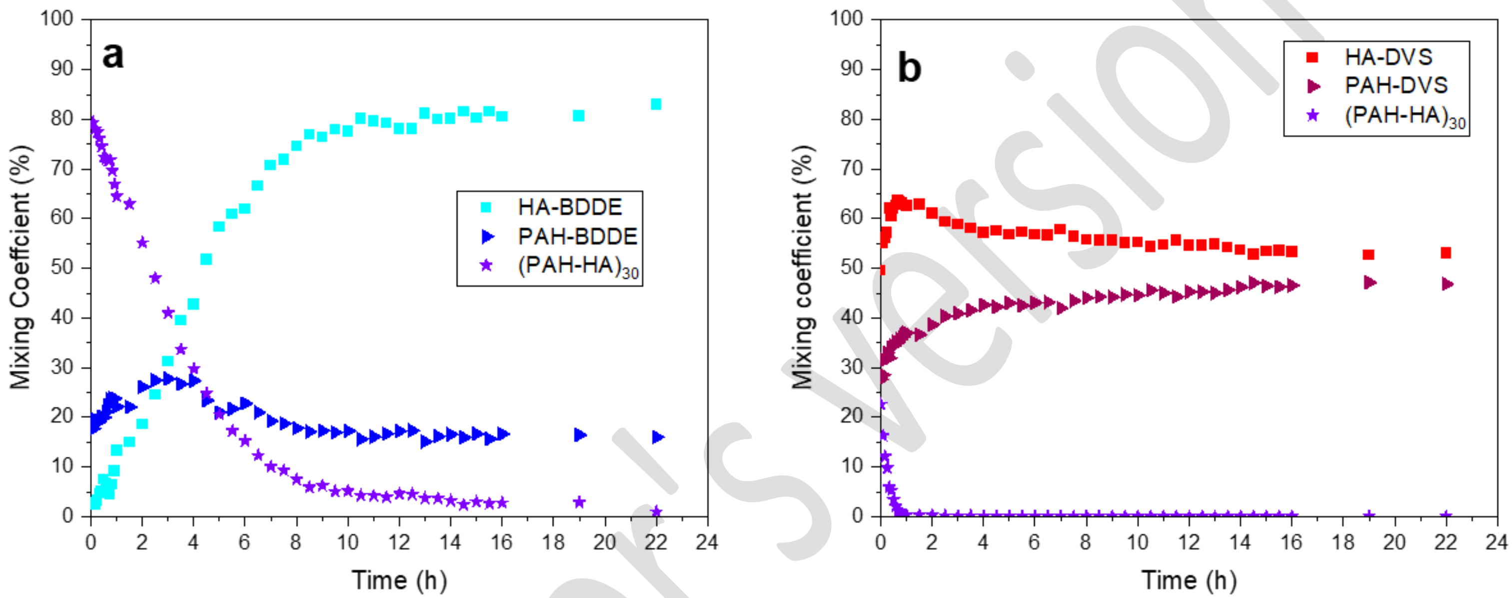

Figure 7. Time-evolution of the mixing coefficients estimated from the ATR-FTIR spectra for (a) (PAH-HA)30 (violet stars), HA-BDDE hydrogel (light blue squares), PAH-BDDE hydrogel (blue triangles) and (b) (PAH-HA)30 (violet stars), PAH-DVS hydrogel (dark red triangles) and HA-DVS (red squares) during crosslinking of $(PAH\text{-}HA)_{30}$, PAH and HA with (a) BDDE or (b) DVS. Mixing coefficients of every component were determined according to BPSS analysis using the ATR-FTIR spectra of each component as known spectroscopic sources (i.e. $(PAH\text{-}HA)_{30}$, HA-BDDE hydrogel and PAH-BDDE hydrogel, or PAH-DVS hydrogel and HA-DVS).